

Received 19 April 2023, accepted 6 May 2023, date of publication 10 May 2023, date of current version 16 May 2023.

Digital Object Identifier 10.1109/ACCESS.2023.3274732

RESEARCH ARTICLE

Power Quality Disturbances Detection and Classification Based on Deep Convolution Auto-Encoder Networks

PORAS KHETARPAL¹, NEELU NAGPAL², (Senior Member, IEEE),
MOHAMMED S. AL-NUMAY³, (Senior Member, IEEE),
PIERLUIGI SIANO⁴, (Senior Member, IEEE),
YOGENDRA ARYA⁵, (Senior Member, IEEE),
AND NEELAM KASSARWANI²

¹Information Technology Department, Bharati Vidyapeeth's College of Engineering, Delhi 110063, India

²Electrical and Electronics Engineering Department, Maharaja Agrasen Institute of Technology, Delhi 110086, India

³Electrical Engineering Department, College of Engineering, King Saud University, Riyadh 11421, Saudi Arabia

⁴Department of Management and Innovation Systems, University of Salerno, 84084 Fisciano, Italy

⁵Department of Electrical Engineering, J. C. Bose University of Science and Technology, YMCA, Faridabad 121006, India

Corresponding authors: Pierluigi Siano (psiano@unisa.it) and Neelu Nagpal (nagpalneelu1971@ieee.org)

The work of Mohammed S. Al-Numay and Pierluigi Siano was supported by the Distinguished Scientist Fellowship Program, King Saud University, Riyadh, Saudi Arabia.

ABSTRACT Power quality issues are required to be addressed properly in forthcoming era of smart meters, smart grids and increase in renewable energy integration. In this paper, Deep Auto-encoder (DAE) networks is proposed for power quality disturbance (PQD) classification and its location detection without using complex signal processing techniques and complex classifiers. In this technique, Gabor filter is used to extract a set of general Gabor features from the convolution of PQD image. Subsequently, through sparse based DAE network, essential and optimal features are extracted and learnt which are used by a simple classifier (SoftMax) to classify the PQD type. Furthermore, the temporal information of the PQD is obtained using the PQD image to correctly locate the disturbance's initiating and terminating instants. The proposed DAE network has the benefits of Deep Learning-based networks in terms of automatic feature selection, but it requires smaller data sets. The issue of obtaining optimised, robust, and strong features from the PQD signal is thus resolved. Excellent classification accuracy of PQD is obtained with appropriate network parameter setting of the proposed DAE network. The proposed technique is compared with three other methods i.e. support vector machine (SVM), stacked auto-encoder (SAE) and principal component analysis (PCA) for PQD classification by implementing all the four techniques on python platform using the same data set. It has an overall classification accuracy of more than 97% at a signal to noise ratio (SNR) of 20dB, which is on the higher side when compared to other methods of PQD detection under noisy environment. Additionally, this method requires less computation time with the same data set than alternative approaches like SVM. Thus, the proposed method outperforms existing methods for PQD classification and detection of single disturbance and multi-disturbance in terms of greater accuracy and reduced computation complexity and computation time.

INDEX TERMS Power quality monitoring, power quality disturbance, deep auto-encoders, optimal feature extraction, power quality event detection.

The associate editor coordinating the review of this manuscript and approving it for publication was Nagesh Prabhu .

I. INTRODUCTION

A. BACKGROUND AND LITERATURE SURVEY

With the advances in electrical and electronic devices and increase in the use of non-linear power electronics-based devices (converters, flexible AC transmission system (FACTS) devices, etc.) and non-linear loads (Variable frequency drives), different power quality (PQ) issues or disturbances are often encountered in the power system. This causes various issues resulting in reduced efficiency of the devices to damage the instrument in case the disturbance is severe. Hence, accurate and efficient monitoring of these PQDs become essential. The emerging smart grid trends with smart meters requires continuous monitoring and detection of PQDs from economic and technical point of view [1]. General PQ issues include voltage variations which are momentary (voltage sag, voltage swell, voltage interruptions, etc.), harmonics, oscillatory transients and their combinations. In addition to IEC 61000-2-5:1995, IEC 61000-2-1: 1990 standards, an IEEE work group 1159-2019 [2] has compiled a list of power quality related definitions and mentions the relevant standards for PQDs. These standards are summarized along with main PQ events as mentioned in [3]. Further, a comprehensive state-of-the-art for different detection and classification techniques of PQDs along with main international standards such as IEC 61000 and EN 50160 have been presented [4]. The general procedure of classifying PQDs involves three major steps: segmentation, feature extraction, and classification [5]. The presence of a PQD signal is identified in the segmentation section, and the disturbance component is extracted from the normal power signal. The transient component is detected, and the disturbance is separated. Following that, in the feature extraction section, various signal processing techniques such as Wavelet transform (WT), S transform (ST), Hilbert Huang transform (HHT), and others are used to extract optimal, strong, and non-redundant features from the power disturbance signal. The disturbance signal is decomposed in WT, yielding multiple signals with varying resolution levels. Detailed version of disturbance signal is obtained in this process to get the features [6]. ST has advantage of multi-resolution analysis (like WT) and uses frequency variables like that of Fourier Transform (FT) [7]. Empirical mode decomposition (EMD) method is used to disintegrate the power disturbance signal in HHT followed by the analysis using Hilbert transform (HT) [8]. Finally, in the classification process, the optimal features of the disturbance is classified using a suitable classifier [9]. SVM, Artificial Neural Network (ANN) etc. are among popular classifiers for PQD classification. ST has been used in [10], [11], [12], and [13], WT in [14], [15], and [16], HHT in [17] and [18] as the feature extraction technique for PQD signal. In [16], [19], [20], and [21] SVM and in [10], [22], [23], and [24] ANN based technique is used for classification purpose of PQD. It is inferred from [25] that better results of classification can be obtained with suitable pairing of signal processing technique and artificial intelligence (AI) based classifiers. Accurate classification of PQD can be possible

with the selection of optimal features from the set of features obtained from the power disturbance signal [26]. From the set of features, Some of these are ignored to get accurate and fast classification. After feature extraction, a optimal feature selection (OFS) model has been used for extracting optimal features from the feature set to remove redundant features and improve classification accuracy and computation time. The developing field of deep learning (DL) addresses the issue of optimal feature extraction and classification jointly to make the process optimized and rich features are learnt automatically from the feature set [27], [28].

The application of DL in the field of image processing has discovered low level structures as well as mid-level structures of images such as edges and shapes [29]. In this way, features extracted by DL networks perform exceptionally well for feature extraction in the presence of noise, outperforming hand-engineered features for classification [30]. Nevertheless, DL-based approaches necessitate large data sets, expensive training, and long training time. In this proposed work, a DL-based auto-encoder technique is used to learn optimized, robust, and strong features from a PQD image, requiring a smaller data set than other DL learning-based methods. It also does not necessitate complex signal processing or machine learning based classification techniques, as previously discussed. As a result, the proposed PQD classification technique requires lesser time and computation effort. A neural network model known as autoencoder (AE) that encodes the high dimensional data and then decodes the compressed version and reconstructs the input could be used to compress data [31]. Multiple layers of AE forms SAE or DAE, a deep neural network. DAE can extract essential and rich features from the images easily which could be classified through a classifier with good accuracy. Rich features are learned during the reconstruction process, and after the training process, the decoding part is discarded, and the features can be used for classification of PQD data or images.

B. PROPOSED WORK

In this paper, Gabor filters are used to extract features from PQD images, and an improved deep convolution autoencoder for PQD image classification is designed using convolution to select strong features. The convolution layer aids in the acquisition of features, after which DAE easily discriminates and learns the rich and essential features, resulting in improved classification accuracy. These strong features are then used with a Softmax classifier to classify PQD types. Following the model's training with noisy PQD images, this method also classifies noisy PQD.

The major contribution of the research is highlighted as below:

- Gabor features are extracted from simple and complex PQD images without noise and with noise at different levels, and optimal and strong features are learned using a deep neural network with a sparse auto-encoder. Gabor features are being used for the first time for PQD classification.

- The proposed DAE network can correctly classify the type of PQD in the images and also accurately determine the location of the disturbance in the PQD image. Hence, temporal information of the PQD can also be determined accurately.
- Excellent classification accuracy of PQD is achieved by appropriate network parameter setting. The features obtained through the DAE network are powerful and outperforms the handcrafted features used without DAE network. Also, less computation time is required using this method with the same data set as compared with other popular methods like SVM.
- DAE network requires less data set as compared to deep learning-based architectures and also does not require complex signal processing techniques like wavelet, FFT etc. hence, it has benefits of deep learning-based networks which are obtained with comparatively smaller data sets.

The rest of this paper is structured as follows. In Section II, the proposed convolution based deep neural network is presented in detail. In section III, PQD data analysis along with data set generation and parameter selection for the proposed deep neural network is given. Section IV, presents the experiments, results and discussions in detail. Finally, the conclusion is summarized in Section V.

II. PROPOSED METHOD

This paper proposes a new PQD classification and detection method using image processing and neural networks-based auto-encoders. This auto-encoder is based on deep learning for robust and strong feature learning. Firstly, through simulation fifteen types of PQD signals are generated. These PQD signals are converted into images. Fig. 1 represents the block diagram to depict the whole process of detection and classification of PQD. Convolution is done for the PQD image with Gabor filter to obtain a set of original Gabor features. These features are then passed through into a DAE neural network, which is trained to learn optimal, strong, and non-redundant features. The DAE network is trained with supervised learning. SoftMax classifier is then used for classification of PQD. For correct detection of temporal information (starting time and ending time) of the disturbance in the image, the image is first converted to grey image (refer Fig. 1). According to [32], grey images reflect the presence and type of PQD in the image. If grey intensity of the PQD image is considered, the grey intensity of the region around sag or voltage interruption is found be darker than the normal part of the signal image. Similarly, the intensity of grey are is found to be lighter than the corresponding part of the signal image for voltage swell. As a result, the beginning and end of this intense section are used to pinpoint the exact location of PQD in the image.

A. DAE NETWORK

In this section, the deep neural network having DAE for PQD image classification is proposed. The deep network is

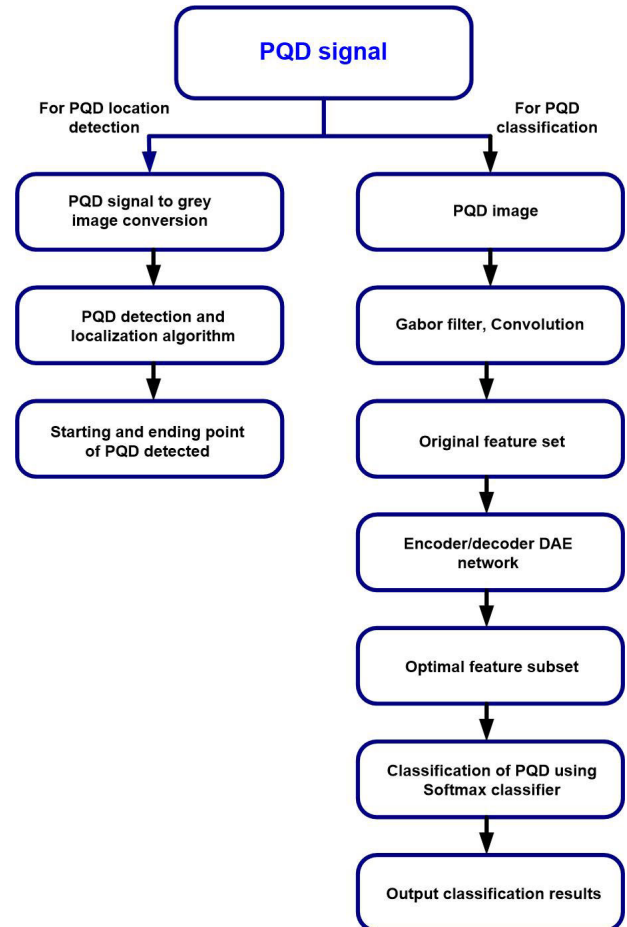


FIGURE 1. Proposed PQD classification and Detection Framework Using DAE Networks and Gabor Filter.

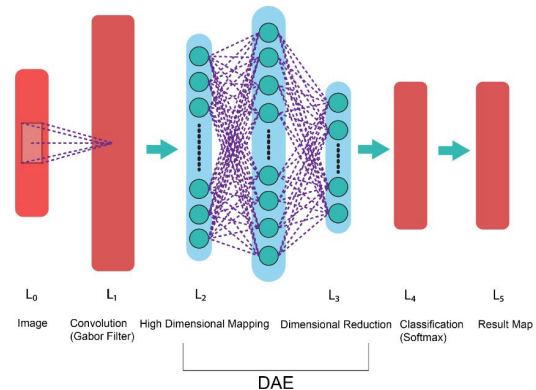


FIGURE 2. Proposed DAE network for PQD classification.

composed of five layers, as shown in Fig. 2. The process is divided into three steps: texture analysis, feature optimization and classification.

1) TEXTURE ANALYSIS

The PQD classification requires extraction of the texture features from PQD images using Gabor filter as convolutional

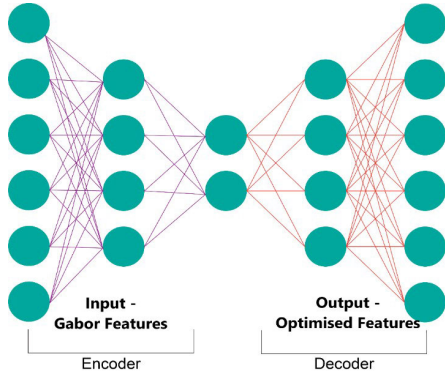


FIGURE 3. Layers of deep neural network as encoder and decoder.

unit. Gabor filter is a type of Gaussian kernel function that function similarly to band-pass filter and can be tuned in terms of central frequency, bandwidth, and orientation. [34]. In case of unsupervised texture, segmentation Gabor filter has the ability to perform well [33]. In Fig. 2, L_0 and L_1 layer could be considered for texture analysis. Given the PQD image P , the mean and variance is computed below.

$$O_1(x, y) = \frac{1}{(2m + 1)^2} \sum_{i=-m}^w \sum_{j=-m}^m P(x + i, y + j)$$

$$O_2(x, y) = \frac{1}{(2m + 1)^2} \sum_{i=-m}^w \sum_{j=-m}^m [P(x + i, y + j)^2 - O_1(x + 1, y + j)]^2 \quad (1)$$

where x and y represent the positions of the pixels in the PQD image, $2m + 1$ represents the window size of the filters, $O_1(x, y)$ represents the mean, and $O_2(x, y)$ represents the variance.

Multi-scale and multi-directional features of the PQD in the frequency domain are obtained with Gabor transform which is similar to Fourier transform combined with Gauss function. The two-dimensional Gabor filter is presented as:

$$G(x_0, y_0, \omega_0, \theta) = \frac{1}{2\pi\sigma^2} \exp\left(-\frac{x_0^2 + y_0^2}{2\sigma^2}\right) [e^{j\omega_0 x_0} - e^{-\frac{\omega_0^2 \sigma^2}{2}}] \quad (2)$$

Also, with $x_0 = x\cos\theta + y\sin\theta$ and $y_0 = -x\sin\theta + y\cos\theta$, centre frequency of the filter is represented by ω_0 . Standard deviation of the Gauss function is represented by σ . Orientation of the Gabor filter is represented by θ . $e^{-\frac{\omega_0^2 \sigma^2}{2}}$ represents the direct current compensation and $e^{j\omega_0 x_0}$ represents the alternating current component. Convolution of the PQD image, $P(x, y)$ with Gabor filter gives multi-scale features of the PQD image. The image is convolved with the Gabor filters present in the first layer which are its convolutional units. The original image is decomposed into multiple filtered images. Each image has some spectral information and hence, texture features are obtained as a multidimensional matrix of

features. To overcome speckle noise effects and reduce computation complexity average pooling is used after obtaining the features. The most important advantage of Gabor filters is their invariance to rotation, scale, and translation [35], [36]. Ten Gabor filters in five scales and eight orientations are applied in the layer L_1 and PQD images used in this present experiments are of size 640×480 pixels. Hence, the dimension of the feature vector is $640 \times 480 \times 10 = 3,072,000$. Due to the high correlation of adjacent pixels in the image, the feature images are down sampled. The proposed work has used a down sampling or feature reduction factor of four hence, size of the feature vector would have a size of $3,072,000/4 = 768000$. Many of these features are not required for good classification accuracy as a large number of features reduces accuracy and consumes an excessive amount of computation time. After application of DAE network, a vector of 8 essential features are obtained. In the following step, feature optimization is used to learn the best, compact, strong, and non-redundant feature set to be used for PQD classification.

2) FEATURE LEARNING

After obtaining the texture features, important distinct and rich features are learnt using two sparse autoencoders in the network. In Fig. 2, layer L_2 and L_3 correspond for the feature extraction part as high dimensional mapping part (encoder) and low dimensional mapping part (decoder) respectively. In sparse encoders, the hidden layers are penalized for activation hence, smaller number of hidden units are activated [37], [38]. The reconstruction error is minimized between the input data and output data of encoder and decoder unit of sparse encoder respectively. Fig.3 shows encoder and decoder based neural network layer. In encoding step, a linear mapping is used with nonlinear activation function to represent an input, where n represent the n^{th} layer of the encoder and is represented as $z_i^n = f_n(W_n x_i^n + b_n)$. The decoding in the decoder step is given by running the stack in reverse order and reconstructed output is obtained as $\hat{x}_i^n = g_n(W_n z_i^n + \hat{b}_n)$ Weight matrices of encoder and decoder part are represented by W_n and \hat{W}_n for the layer respectively. Similarly, the weight biases for encoder and decoder units are represented by b_n and \hat{b}_n respectively. Also, encoder and decoder functions are represented by $f_n(\cdot)$ and $g_n(\cdot)$, and these functions are normally tanh or sigmoid function. The loss function which is optimized for the n^{th} layer autoencoder is given below.

$$J_{SAE}(W_n, b_n, \hat{W}_n, \hat{b}_n) = J(W_n, b_n, \hat{W}_n, \hat{b}_n) + \sigma \sum_{j=1}^{i_n} KL(\beta || \hat{\beta}_j) \quad (3)$$

where, $J_{SAE}(W_n, b_n, \hat{W}_n, \hat{b}_n)$ is the loss function which does not include sparse constraint and represented as:

$$J_{SAE}(W_n, b_n, \hat{W}_n, \hat{b}_n) = \arg \min_{W_n, b_n, \hat{W}_n, \hat{b}_n} \sum_{i=1}^k \|x_i^n - \hat{x}_i^n\|^2 + \frac{\mu}{2} \|W_n\|_F^2 \quad (4)$$

where, μ denotes the parameter for weight decay, total number of samples are denoted by k . Also, hidden values of $(n - 1)^{th}$ layers acts as the inputs for the n^{th} layer, i.e., $x_i^n = z_i^{n-1}$, Sparsity penalty is represented by α . Count of hidden neurons of n^{th} layer is represented by i_n . Further, $KL(\beta||\hat{\beta}_j)$ represents Kullback–Leibler divergence ranging between β and $\hat{\beta}_j$ defined as:

$$KL(\beta||\hat{\beta}_j) = \beta \log \frac{\beta}{\hat{\beta}_j} + (1 - \beta) \log \frac{1 - \beta}{1 - \hat{\beta}_j} \quad (5)$$

where, β represents the sparsity parameter. k^{th} hidden unit average activation over the sample set is represented by $\hat{\beta}_j$ i.e., $\hat{\beta}_j = \frac{1}{K} \sum_{i=1}^K f_{n,j}(x_i^n)$.

Two sparse autoencoders are used one after the other. The sparse encoder (first one) is designed with number of hidden units greater than that of the input layer so that linear features are obtained. After the first encoder, the second encoder is designed in such a way such that the number of hidden units are lesser than the input so that the feature set dimension is reduced. After the layers of encoders, SoftMax classifier is applied [39]. The neural network's raw output is finally converted into probabilities by the SoftMax classifier, and classification is completed. The SoftMax classifier normalizes the probability values of output received from the autoencoder. The learning rate of 0.6 is chosen after repeated simulation tests. The deep neural network develop needs to be initialized first, so, ReLU (rectified linear activation function) function is used to initialize the deep neural network. After assigning weights, biases are optimised jointly. Method of gradient descent is applied to update the autoencoder and classification layer parameters.

3) CLASSIFICATION

The final layer $L4$, or the SoftMax classifier, classifies the image or images after the biases and weights have been optimised. Softmax classifier is a ML based algorithm. It is a supervised learning algorithm that is used for multiple classes of classification. It assigns probability distribution (PD) to each class. The class with highest probability is given a normalized value of '1' as PD and PD of other classes are scaled accordingly. This classifier works with PD and is preferred here due to its faster execution time for multiple class based classifiers. The classifier results in high accuracy of classification. It computes the probability of the image sample x_i belonging to the o^{th} class.

$$p(y_i = o|x_i; W_4, b_4) = \frac{e^{W_4^{(o)T} x_i + b_4^{(o)}}}{\sum_{j=1}^z e^{W_4^{(j)T} x_i + b_4^{(j)}}} \quad (6)$$

The weights portion and biases portion in the o^{th} class is denoted by $W_4^{(o)}$ and $b_4^{(o)}$ respectively. Total number of classification categories is represented by z . We get maximal probability of the sample x_i and hence, the classification label

is determined through equation:

$$\text{class}(x_i) = \arg \max(t = 1, \dots, c) p(y_i = o|x_i; W_4, b_4) \quad (7)$$

III. PQD ANALYSIS

In this section, PQDs are generated using MATLAB environment to develop required data set and then, the data is converted to images. Further, the analysis of the disturbances is carried out following the process proposed in section II.

A. PQD DATASET GENERATION

A dataset of PQDs is required for proper PQ disturbance classification. The availability of PQD data in large numbers is difficult to obtain since the occurrence of all types of PQ disturbances is not guaranteed, and the location and time are also not fixed. As a result, synthetic PQDs data is widely used for training neural network layers [40]. PQDs are simulated in MATLAB using numerical models imitating the PQ disturbances and these simulated PQDs are very close to the real PQ disturbances that could be used for training and testing of deep neural networks. Further to accommodate the modelling uncertainty from real signal, white Gaussian noise (WGN) is added to these signals that is a general practice in power system modelling [41], [42], [43]. Single PQD as well as multiple PQDs are developed using the numerical models [44] which are presented in Table 1.

Fifteen types of PQD named as standard voltage signal (C1), voltage sag (C2), voltage swell (C3), voltage interruption (C4), voltage harmonics (C5), transient oscillation (C6), voltage flicker (C7), impulse transient (C8), voltage notch (C9), voltage sag with harmonics (C10), voltage swell with harmonics (C11), voltage sag with oscillation (C12), voltage swell with oscillation (C13), voltage sag with harmonics and oscillation (C14), voltage swell with harmonics and oscillation (C15) are developed through the numerical modelling. The signal is chosen that is generated with fundamental frequency of 50 Hz and sampling rate of 3200 Hz. Length of 10 cycles is chosen for each signal. The single dimension PQD signal data is obtained in CSV format which is then converted to two-dimensional image with the use of Matplotlib library of python. Fig. 4 shows some of the PQD waveform images generated through process. Fig. 4(a) presents normal 50Hz sinusoidal voltage. Fig. 4(b) presents an oscillatory transient (OT). OT is a frequency change in voltage with both positive and negative polarity values. Fig. 4(c) presents sag in voltage waveform. Sag is a fall in RMS value of normal sinusoidal voltage signal ranging between 0.1 pu and 0.9 pu with a time period ranging between 0.5 cycles to 1 minute. Fig. 4(d) is swell in voltage signal. Swell is a rise in RMS voltage which is above 1.1 pu and exists for a duration ranging from 0.5 cycles to 1 minute. Fig. 4(e) is interruption in voltage signal. In this the voltage supply falls below 0.1 pu for time duration which is less than 1 minute. Fig. 4(f) is flicker in voltage and is continuous and fast variations in voltage waveform.

TABLE 1. Numerical modeling of the simulated PQ disturbances [21].

PQ Event	Numerical Model	Parameters
Pure sine (C1)	$V(t) = A \sin(\omega t)$	$A=1$ (pu), $\omega = 2\pi 50$ rad/s
Sag (C2)	$V(t) = (1 - \alpha(u(t - t_1) - u(t - t_2))) \sin \omega t$	$0.1 \leq \alpha \leq 0.9, T \leq (t_2 - t_1) \leq 9T$
Swell (C3)	$V(t) = (1 + \alpha(u(t - t_1) - u(t - t_2))) \sin \omega t$	$0.1 \leq \alpha \leq 0.8, T \leq (t_2 - t_1) \leq 9T$
Interruption (C4)	$V(t) = \alpha(u(t - t_1) - u(t - t_2)) \sin \omega t$	$0.9 \leq \alpha \leq 1.0, T \leq (t_2 - t_1) \leq 9T$
Harmonics (C5)	$V(t) = \alpha_1 \sin(\omega t) + \alpha_3 \sin(3\omega t) + \alpha_5 \sin(5\omega t) + \alpha_7 \sin(7\omega t)$	$0.05 \leq \alpha_3, \alpha_5, \alpha_7 \leq 0.15, \sum \alpha_i^2 = 1$
Oscillatory transient (C6)	$V(t) = \sin \omega t + \alpha e^{\frac{(t-t_1)}{\tau}} \sin \omega_n(t - t_1)(u(t_2 - u(t_1)))$	$(0.1 \leq \alpha \leq 0.8, 0.5T \leq (t_2 - t_1) \leq 3T$ $8 \text{ ms} \leq t \leq 40 \text{ ms}, 300 \leq f_n \leq 900 \text{ Hz} \leq \tau$
Flicker (C7)	$V(t) = (1 + \alpha_f \sin(\beta \omega t)) \sin \omega t$	$0.1 \leq \alpha_f \leq 0.2, 5 \leq \beta \leq 20 \text{ Hz}$
Impulse transient (C8)	$V(t) = \sin \omega t + \text{sign}(\sin \omega t) \times [\sum_{n=0}^9 K \{u(t - (t_1 + 0.02n)) - u(t - (t_2 + 0.02n))\}]$	$0.1 \leq K \leq 0.4, 0 \leq t_1, t_2 \leq 0, 5T$ $0.01 \leq (t_2 - t_1) \leq 0.05T$ $0.1 \leq \alpha_f \leq 0.2, 5 \leq \beta \leq 20 \text{ Hz}$
Notch (C9)	$V(t) = \sin \omega t - \text{sign}(\sin \omega t) \times [\sum_{n=0}^9 K \{u(t - (t_1 + 0.02n)) - u(t - (t_2 + 0.02n))\}]$	$0.1 \leq K \leq 0.4, 0 \leq t_1, t_2 \leq 0, 5T$ $0.01 \leq (t_2 - t_1) \leq 0.05T$
Sag with Harmonics (C10)	$V(t) = (1 - \alpha(u(t - t_1) - u(t - t_2))) \alpha_1 \sin(\omega t) + \alpha_3 \sin(3\omega t) + \alpha_5 \sin(5\omega t) + \alpha_7 \sin(7\omega t)$	$0.1 \leq \alpha \leq 0.9, T \leq (t_2 - t_1) \leq 9T$ $0.05 \leq \alpha_3, \alpha_5, \alpha_7 \leq 0.15, \sum \alpha_i^2 = 1$
Swell with Harmonics (C11)	$V(t) = (1 + \alpha(u(t - t_1) - u(t - t_2))) \alpha_1 \sin(\omega t) + \alpha_3 \sin(3\omega t) + \alpha_5 \sin(5\omega t) + \alpha_7 \sin(7\omega t)$	$1.1 \leq \alpha \leq 1.8, T \leq (t_2 - t_1) \leq 9T$ $0.05 \leq \alpha_3, \alpha_5, \alpha_7 \leq 0.15, \sum \alpha_i^2 = 1$
Sag with oscillation (C12)	$V(t) = A[\sin(\omega t - \phi)(1 + \alpha(u(t - t_1) - u(t - t_2))) + \beta e^{-(t-t_3)/\tau} \sin(\omega_n(t - t_3) - \nu)((u(t - t_4) - u(t - t_3)))]$	$1.1 \leq \alpha \leq 1.8T \leq (t_2 - t_1) \leq 9T$ $0.05 \leq \alpha_3, \alpha_5, \alpha_7 \leq 0.15, \sum \alpha_i^2 = 1$
Swell with oscillation (C13)	$V(t) = A[\sin(\omega t - \phi)(1 + \beta(u(t - t_1) - u(t - t_2))) + \beta e^{-(t-t_3)/\tau} \sin(\omega_n(t - t_3) - \nu)((u(t - t_4) - u(t - t_3)))]$	$1.1 \leq \alpha \leq 1.8, T \leq (t_2 - t_1) \leq 9T$ $0.05 \leq \alpha_3, \alpha_5, \alpha_7 \leq 0.15, \sum \alpha_i^2 = 1$
Swell with Harmonics and Oscillations (C13)	$V(t) = (1 - \alpha(u(t - t_1) - u(t - t_2))) \alpha_1 \sin(\omega t) + \alpha_3 \sin(3\omega t) + \alpha_5 \sin(5\omega t) + \alpha_7 \sin(7\omega t)$	$0.9 \leq \alpha \leq 1.0, T \leq (t_2 - t_1) \leq 9T$ $0.05 \leq \alpha_3, \alpha_5, \alpha_7 \leq 0.15, \sum \alpha_i^2 = 1$
Sag with Harmonics and Oscillations (C14)	$V(t) = A[\sin(\omega t - \nu_1) + (-\alpha(u(t - t_1) - u(t - t_2))) + \sum_{n=1}^5 [\alpha_n(\sin(n\omega t - \nu_n) + \beta e^{\frac{(t-t_3)}{\tau}} \sin(\omega_n(t - t_3) - \nu)(u(t - t_4) - u(t - t_3)))]$	$0.9 \leq \alpha \leq 1.0, T \leq (t_2 - t_1) \leq 9T$ $0.05 \leq \alpha_3, \alpha_5, \alpha_7 \leq 0.15, \sum \alpha_i^2 = 1$
Swell with Harmonics and Oscillations (C15)	$V(t) = A[\sin(\omega t - \nu_1) + (\beta(u(t - t_1) - u(t - t_2))) + \sum_{n=1}^5 [\alpha_n(\sin(n\omega t - \nu_n) + \beta e^{\frac{(t-t_3)}{\tau}} \sin(\omega_n(t - t_3) - \nu)(u(t - t_4) - u(t - t_3)))]$	$0.9 \leq \alpha \leq 1.0, T \leq (t_2 - t_1) \leq 9T$ $0.05 \leq \alpha_3, \alpha_5, \alpha_7 \leq 0.15, \sum \alpha_i^2 = 1$

The developed data set contains 1000 images of 15 different types of PQDs. Each image has a resolution of 480 * 640 pixels. For training, 750 images of each PQD type are used, out of which 250 images of each PQD type are used for testing. In addition, images with the same number are generated by adding white Gaussian noise to the PQD data with SNRs of 20dB, 30dB, and 40dB. The proposed model is also trained with noisy PQD images for classification of PQD.

B. PARAMETER SELECTION

The classification accuracy of the proposed deep neural network greatly depends upon its structure and selection of parameter values. As discussed in section II, ten Gabor filters are used for texture analysis with five scales and eight orientations including [0, ($\pi/8$), ($\pi/4$), ($3\pi/8$), ($\pi/2$), ($5\pi/8$), ($3\pi/4$), ($7\pi/8$)] in the layer L_1 to obtain the initial feature set of the PQD image. The original PQD image is convolved with the Gabor filters and decomposed into multiple filtered images. Each obtained image has some spectral information. As a result, a multidimensional matrix of features is obtained. In general, the classification accuracy of a machine learning (ML) model/deep learning model is the ratio of correct classifications made by the model for each class and total number of classifications made for each class. The classification performance of the proposed model is evaluated by the indexes termed as average accuracy (AA) and overall

accuracy (OA). AA is defined as the ratio of the total sum of accuracy of classification for each class and the total number of classes available for classification where as OA of a machine learning based model is defined as the ratio of total number of correct classification predictions made by the machine learning/deep learning model and the total number of classification predictions made by the model.

As discussed in section II-A, average pooling is done after obtaining the set of Gabor features to reduce the complexity of computation and reduce speckle noise effect. Variance filter and mean filter size are used to determine window size of average pooling. Classification accuracy with different values of s is shown in Fig. 5 where, s is ranged from 4 to 20 and this indicates the effect on classification accuracy when window size of the convolution filter is changed. Further, it is worthy to note from the results that if pooling is done appropriately, the effect of noise is limited and also the size of window should not be too large. It is found that when $s = 12$, the performance of the network is found to be satisfactory. Layer L_2 and layer L_3 represent the two layers of DAEs and number of units present in each layer are represented by L_2 and L_3 respectively. The classification accuracy of the deep neural network depends upon the parameters s, L_2 and L_3 . The hyper parameters μ, α , and β are set to 0.005, 0.01, and 0.5 respectively. L_2 and L_3 are set to 90 and 30 respectively. Fig. 6 shows the classification accuracy of the deep neural network with different values of L_2 and L_3 , setting L_2 from 20 to 200 and

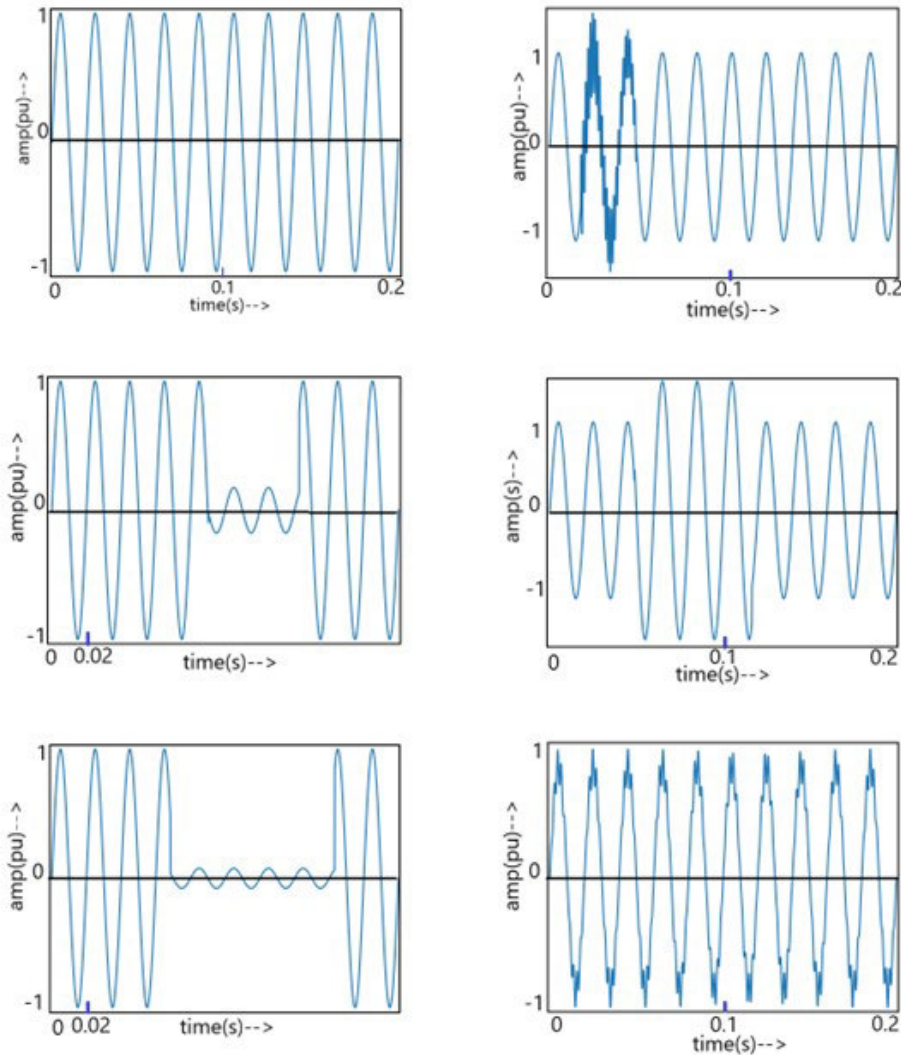


FIGURE 4. PQD images (a) Normal voltage waveform (b) Oscillatory transient (c) Voltage sag (d) Voltage swell (e) Voltage interruption (f) Voltage flicker.

L_3 from 20 to 60. The experiment was executed four times with a set of parameters and mean value was calculated for each case.

The deep neural network performs best when $L_2 = 90$ and $L_3 = 30$ with good OA. Keeping L_4 fixed, the DAE network achieved a good performance when L_2 ranged between 90 and 140. The result indicated that with high-dimensional mapping the classification accuracy could be improved by increasing the value of L_2 , but after increasing L_2 beyond a certain value, it was observed that the performance was not affected much. Hence, it could be concluded that since L_2 is used for high dimensional mapping and L_3 is used for dimension reduction, this abrupt reduction may be responsible for weakening of important information. It is also observed that the value of L_3 should neither be too high and nor too low. Hence, high value of L_3 may lead to overfitting problem in classifier training and low value of L_3 may lead to loss of important

TABLE 2. Classification accuracy computed with different features (in %age).

Class	Pixel(%)	Gabor(%)	GLCM(%)
OA	87.53	95.33	89.53
AA	90.23	99.4	93.66

features. Hence L_3 was chosen to be between 25 to 40 and corresponding values of L_2 was found out to be between 90 and 140.

IV. RESULTS AND ANALYSIS

A DAE network is created as described in section II, and parameters are configured as described in section III-B. After selecting and setting the perfect parameters for DAE network ($s=12, L_2=90$ and $L_3=30$), the experiments are performed.

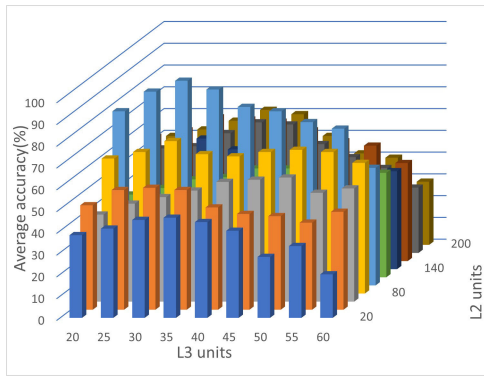


FIGURE 5. Comparison of classification performance when window size(s) of Gabor filter is changed.

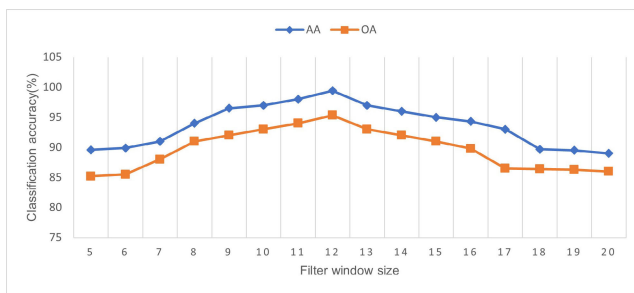


FIGURE 6. Comparison of classification performance when L_2 and L_3 units are varied.

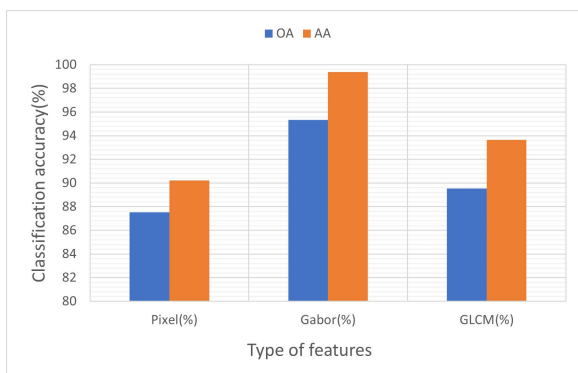


FIGURE 7. Classification accuracy comparison of different features.

25% percent of the units of L_2 layer and 25% of the units of L_3 layer are dropout to control the overfitting problem. Gabor filter is used for feature extraction in L_1 layer. For proper analysis, many different features are learnt which are then compared in Table 2 for their classification accuracy after learning process. The features considered for analysis are pixel features which are learnt from the PQD original image, Gabor features from L_1 layer and grey level co-occurrence matrices (GLCM) features from L_1 layer. It could be seen from Table 2 that Gabor and GLCM features perform better than the pixel features and Gabor features lead to better classification accuracy than GLCM features. Fig. 7 depicts a graphical comparison of OA and AA for the classification

TABLE 3. Average accuracy of PQD classification of proposed work with different SNR ratios.

Class	Accuracy (%)	Accuracy(%)	Accuracy(%)	Pure (%)
	20dB	30dB	40dB	
C1	98.5	98.99	99	99.7
C2	98.5	98.85	99.33	99.5
C3	98.33	98.67	98.99	99.33
C4	97.93	98.5	99	99.8
C5	97.67	99	99.33	99.66
C6	98.5	99	98.33	99
C7	99.33	99.5	99.8	99.97
C8	96.3	99.33	99.66	100
C9	98.33	99.5	99.7	100
C10	97.65	98	98.33	99
C11	98	98.33	98.5	99
C12	97.99	98.5	98.99	99
C13	98.53	98.78	99	99.33
C14	97.73	98.33	98.66	98.9
C15	96.7	97.15	97.33	98.81
Avg. Acc	97.99	98.69	98.93	99.4

of PQD using pixel, Gabor, and GLCM features. Hence, the use of Gabor features are preferred in this proposed work.

A. PERFORMANCE ANALYSIS UNDER NOISY PQDs

The efficacy of the proposed method to classify single and multiple PQDs under different noise conditions such as without noise and with noise at different levels. PQD signals with 20dB, 30dB and 40dB of noise were generated and the training and testing of the proposed model was done considering these conditions. With the incursion of noise in the signal, the quality of PQD images degrades. However, the proposed technique has the ability to extract the strong features of images. The classification accuracy of fifteen different PQDs (refer Table 1) with varying signal to noise (SNR) ratios, such as 20 dB, 30 dB, and noiseless PQD signal, is shown in Table 3. As it could be seen from this Table that although the average classification accuracy (AA) declines as the noise level increases but in the proposed method, PQD images with no noise achieves 99.4% AA, 98.93% AA of PQD with SNR of 20dB, 98.69% AA is obtained for PQD with SNR of 30dB, and 97.99% AA is obtained for PQD with SNR of 40dB using Gabor features. Fig. 8 compares the classification accuracy of PQ events with different values of SNR as mentioned in Table 3. The experimental results mentioned in this table indicates the efficacy of the proposed model in classifying PQD with better accuracy, even under noisy conditions.

B. PERFORMANCE COMPARISON

A comparison of the proposed work is carried out with three other common approaches, SVM [34] and SAE [37] and Principal component analysis (PCA). We have implemented all the four PQD classification techniques on python platform and used the same data set to conduct extensively comparative experiments to verify the superiority of the proposed framework. SVM is a well-established method that can work using limited data sets. We have applied kernel SVM using sigmoid function to convert non-linear data into simple linear data. Support vector classifier (SVC) is used for the classification



FIGURE 8. Classification accuracy of PQ events (%) with different values of SNR.

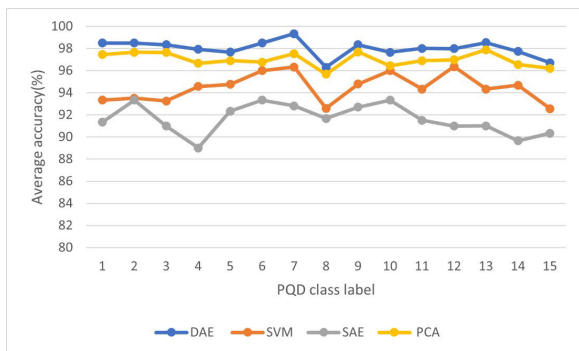


FIGURE 9. Classification accuracy comparison different methods for each class of PQ event.

purpose. Regularization constant (C) is obtained by using grid search technique. In the above comparison method, independent component analysis (ICA) is applied to the feature set obtained after convolution with Gabor filter to reduce the number of features and select good features. 75% of the samples are taken as training samples and rest 25% as testing samples. In SAE method, Gabor features are not considered and features are learnt directly through a single layer of autoencoder and classification is done by SoftMax classifier. In PCA based method, the PQD image is convolved with the Gabor filter and PCA is used for feature selection rather than sparse autoencoder with same data set. The results are shown in Table 4 and Table 5. Table 4 gives the comparison of overall classification accuracy (OA) for 15 different classes and execution time of the proposed method with SVM, SAE, and PCA based methods. It could be observed from this table that the proposed method outperforms the other three methods in terms of overall classification accuracy and execution time. The proposed method's PQD classification accuracy (AA) for each class is compared in Table 5 with methods based on SVM, SAE, and PCA for 20 dB SNR. This table and corresponding Fig. 9 show that, in comparison to the other three alternatives, the proposed method provides good PQD classification accuracy for each class in the presence of noise with a 20 dB SNR.

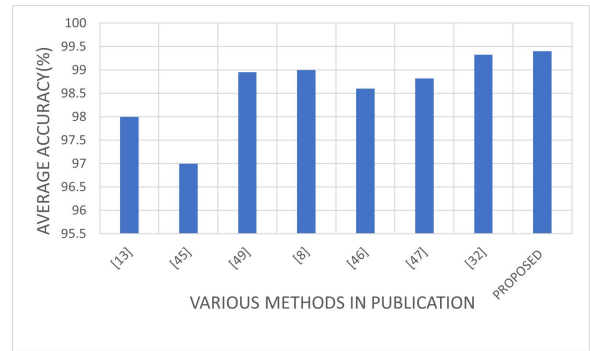


FIGURE 10. Comparison of recent PQD classification techniques with the proposed method.

TABLE 4. Classification accuracy (OA) and time of computation (s) comparison of different methods with different SNR ratio.

Class	DAE	SVM	SAE	PCA
Pure (%)	99.4	95.45	93.33	98.66
20DB (%)	97.99	94.48	91.61	96.65
30DB (%)	98.69	94.75	92.33	97.64
40DB (%)	98.93	95.33	93.12	97.99
Time(s)	0.013	0.024	0.023	0.021

TABLE 5. AA of different methods for each class of PQ event.

Class	AA DAE	AA SVM	AA SAE	AA PCA
	20dB(%)	20dB(%)	20dB(%)	20dB(%)
C1	98.5	93.33	91.33	97.45
C2	98.5	93.5	93.33	97.66
C3	98.33	93.25	90.99	97.64
C4	97.93	94.56	89	96.66
C5	97.67	94.76	92.33	96.89
C6	98.5	95.99	93.33	96.77
C7	99.33	96.33	92.8	97.53
C8	96.3	92.58	91.66	95.67
C9	98.33	94.78	92.7	97.68
C10	97.65	95.99	93.33	96.43
C11	98	94.33	91.5	96.89
C12	97.99	96.35	90.99	96.98
C13	98.53	94.33	91	97.87
C14	97.73	94.67	89.66	96.54
C15	96.7	92.55	90.33	96.2
AA	97.99	94.48	91.61	96.65

It could be seen that our proposed method for PQD classification (DAE) performs far better than the three methods. According to the results, with and without different levels of noise, features extracted automatically through DAE perform better than features extracted automatically through ICA in SVM method and automatic feature learning in simple SAE method. In addition, the classification process takes less computational time than all the three methods. It is observed that proposed DAE network selects and learns more discriminating features from the feature sets as compared to other three methods.

Table 6 and Fig. 10 compares various latest methods for PQD classification available. In [13], multi-resolution ST is used for optimal feature extraction from PQD signal and

TABLE 6. Comparison of recent PQD classification techniques with the proposed method.

Ref. paper	Feature Extraction Method	Classifier Type	Data Type	With Noise	No.of PQ Events	Total Efficiency
[8]	HHT	Extreme learning machine (WBELM)	Real and Artificial	Yes	16	95.5 % and 99 %
[13]	ST	Fuzzy Logic	Artificial	yes	14	98 %
[15]	DWT	SVM	Artificial	yes	11	98.95%
[32]	-	Random Forest (RF)	Artificial	Yes	9	99.33 %
[45]	S-transform Variant	Support Vector Machines (DAG-SVMs)	Artificial	Yes	9	97%
[46]	Sparse Auto Encoder (SAE)	Independent Component Analysis (ICA)	Artificial	No	> 7	98.6%
[47]	Variational Mode Decomposition (VMD)	Kernel Extreme Learning Machine (KELM)	Artificial	No	15	98.82%
[48]	WT	NN	Artificial	Yes	7	94.93%
[49]	WT	SVM	Artificial	Yes	8	98.95%
[50]	Ensemble Empirical Mode Decomposition (EEMD)	Rank Wavelet Support Vector Machine (RWSVM)	Artificial	Yes	8	92.8%
Proposed Method	Deep Auto Encoder	Softmax classifier	Artificial	Yes	15	99.4%

then simple fuzzy logic-based classifier is used for classification. A good classification accuracy is obtained which is around 98%. Multi-resolution ST technique used here is complex since it is using convolution along with Fast Fourier Transform to obtain a complex feature matrix whereas in the proposed method, simple Gabor features are extracted without any complex mathematical algorithm and then efficient features are learnt using DAE giving an average accuracy of 99.4%. In [45] a modified ST technique is used for efficient feature extraction and SVM variant is used for classification of nine types of PQD. A run time of 13.4 ms is reported for the proposed method (excluding training and testing times) whereas proposed method takes 13 ms of run time with greater accuracy. In [15], discrete wavelet transform (DWT) is clubbed with SVM as a classifier for 11 types of PQD classification. As compared to the proposed method, DWT as a feature extraction technique along with SVM as a classifier is complex. Classification accuracy of 98.95% is achieved which is less than that of proposed method. In [8], HHT along with ELM is applied for the purpose of PQD classification, HHT is fast and advanced signal processing technique, but average run time mentioned is 19 ms which is greater than the proposed technique’s run time, accuracy for both the techniques nearly matches with proposed technique having accuracy on higher side. In [46], ICA is used with SAE along with SoftMax classifier to classify PQDs. ICA is used for feature set extraction and SAE for choosing the right features. As compared, features obtained in the proposed methods are easier to obtain and also higher accuracy is obtained for PQD classification. In [47] VMD is applied with a variant of extreme learning machine, the technique gives very good results and selects optimum features, but its run time is approximately 27.4 ms which is greater than the proposed method which has a run time of 13 ms. In [32], image processing is used for the purpose of PQD classification, PQD

TABLE 7. PQD time detection.

Class label	PQ event	Starting time (s)	Ending time (s)
C6	Oscillatory transients	0.0162	0.0531
C3	Voltage swell	0.0842, 0.143	0.0881, 0.182

image is first processed with three types of image enhancement techniques, features are extracted and then important features are selected based on Gini importance and finally disturbance classification is done with RF classifier with an accuracy of 99.33% for nine types of artificially generated PQDs. Whereas an accuracy of 99.40% is obtained with the proposed method with simple feature extraction and selection process. Important point is that in both the methods, image processing techniques are being used for PQD classification, but the proposed method is less complex and straightforward. It is inferred that the proposed DAE method outperforms all other methods in terms of classification accuracy.

C. PQD TIME DETECTION

Images of the PQ signals are taken in batches and there is one class which denotes normal voltage signal and the rest others have disturbance in between the image batch. The proposed DAE network can classify the type of PQD present in the image along with the starting and ending times of the disturbance. This may be the sudden change or transient that happens in the normal sinusoidal voltage that gives the information regarding the presence with onset and ending times of disturbance in voltage signal. Time detection of PQD is restricted to appearance since when disturbance appears in a normal sinusoidal voltage, the transient that occurs gives the starting point of the PQD. If this PQD is converted to a grey image then the intensity of the grey part after the start and duration of PQD is different from normal sinusoidal voltage

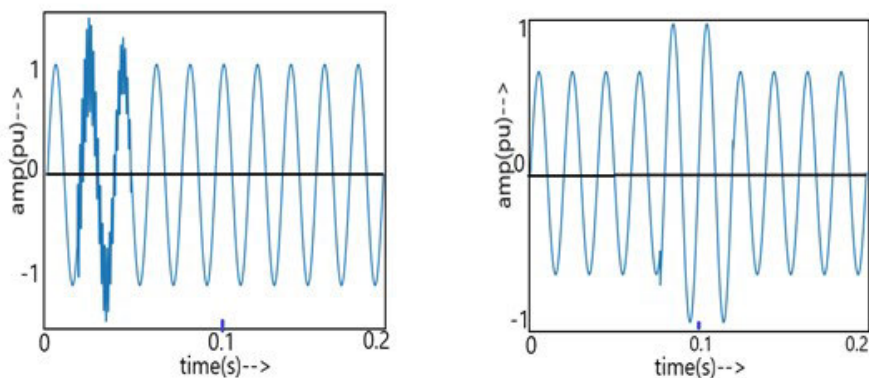


FIGURE 11. PQD images (a) Oscillatory transient (C6). (b) Voltage swell (C3).

grey image. Hence, this difference in grey image intensity gives the starting and ending point of PQD.

For correct detection of temporal information (starting time and ending time) of the disturbance in the image, the image is first converted to a grey image as shown in Fig. 1. According to [32], grey images reflect the presence and type of PQD in the image. If the grey intensity of the PQD image is considered, the grey intensity of the region around sag or voltage interruption is found to be darker than the normal part of the signal image. Similarly, for voltage swell the intensity of grey area is found to be lighter than the corresponding part of the signal image hence, starting and ending of this intense part is used to give the exact location of PQD in the image. The proposed DAE network can classify the type of PQD present in the image along with the starting and ending times of the disturbance. Table 7 gives the starting and ending times of some of the PQD events as shown in Fig. 11.

V. CONCLUSION

This paper has successfully performed PQD classification and occurrence time detection using a new image recognition technique based on an improved deep autoencoder to obtain the best features with minimum data set, less complexity and computation time. In this technique, the redundant and unnecessary features are neglected from the original feature set obtained through convolution using Gabor filter. Subsequently, the optimised features learned through the improved DAE network are used for classification of 15 different types of PQ events, including the normal voltage waveform. The main advantages of the proposed method include: high accuracy classification of real and noisy PQDs, requirement of lesser computation time using this method with the same data set contrarily to other popular methods like SVM, use of Gabor filter to extract features from PQD images hence, complex signal processing techniques are not required, and accurate determination of temporal information (starting and ending time) of the PQD. The proposed model achieves an overall classification accuracy of more than 97% with an SNR of 20dB, which is on the higher side when compared to other popular methods for PQD classification. As a result, it is concluded that the proposed technique has the potential

to identify any problems with power quality quickly and accurately.

REFERENCES

- [1] A. Bose, "Smart transmission grid applications and their supporting infrastructure," *IEEE Trans. Smart Grid*, vol. 1, no. 1, pp. 11–19, Jun. 2010.
- [2] *IEEE Recommended Practice for Monitoring Electric Power Quality*, IEEE Standard 1159-2019, IEEE Std 1159-2009, Aug. 2019, pp. 1–98, doi: 10.1109/IEEESTD.2019.8796486.
- [3] N. Kassarwani, "Performance study of dynamic voltage restorer for mitigation of voltage sags," Ph.D. thesis, Dept. Elect. Eng., NIT Kurukshetra, Kurukshetra, India, 2019.
- [4] G. S. Chawda, A. G. Shaik, M. Shaik, S. Padmanaban, J. B. Holm-Nielsen, O. P. Mahela, and P. Kaliannan, "Comprehensive review on detection and classification of power quality disturbances in utility grid with renewable energy penetration," *IEEE Access*, vol. 8, pp. 146807–146830, 2020, doi: 10.1109/ACCESS.2020.3014732.
- [5] P. Khetarpal and M. M. Tripathi, "A critical and comprehensive review on power quality disturbance detection and classification," *Sustain. Comput., Informat. Syst.*, vol. 28, Dec. 2020, Art. no. 100417, doi: 10.1016/j.suscom.2020.100417.
- [6] S. Santoso, E. J. Powers, and W. M. Grady, "Power quality disturbance data compression using wavelet transform methods," *IEEE Trans. On Power Del.*, vol. 12, no. 3, pp. 1250–1256, Jul. 1997.
- [7] S. ventosa, C. Simon, M. Schimmel, J. J. Danobeitia, and A. Manuel, "The S-transform from a wavelet point of view," *IEEE Trans. Signal Process.*, vol. 56, no. 7, pp. 2771–2780, Jul. 2008.
- [8] M. Sahani and P. K. Dash, "Automatic power quality events recognition based on Hilbert Huang transform and weighted bidirectional extreme learning machine," *IEEE Trans. Ind. Informat.*, vol. 14, no. 9, pp. 3849–3858, Sep. 2018.
- [9] U. Singh and S. N. Singh, "Optimal feature selection via NSGA-II for power quality disturbances classification," *IEEE Trans. Ind. Informat.*, vol. 14, no. 7, pp. 2994–3002, Jul. 2018.
- [10] S. Mishra, C. N. Bhende, and B. K. Panigrahi, "Detection and classification of power quality disturbances using S-transform and probabilistic neural network," *IEEE Trans. Power Del.*, vol. 23, no. 1, pp. 280–287, Jan. 2008.
- [11] I. W. C. Lee and P. K. Dash, "S-transform-based intelligent system for classification of power quality disturbance signals," *IEEE Trans. Ind. Electron.*, vol. 50, no. 4, pp. 800–805, Aug. 2003.
- [12] R. Kumar, B. Singh, D. T. Shahani, A. Chandra, and K. Al-Haddad, "Recognition of power-quality disturbances using S-transform-based ANN classifier and rule-based decision tree," *IEEE Trans. Ind. Appl.*, vol. 51, no. 2, pp. 1249–1258, Mar./Apr. 2015.
- [13] M. V. Chilukuri and P. K. Dash, "Multiresolution S-transform-based fuzzy recognition system for power quality events," *IEEE Trans. Power Del.*, vol. 20, no. 1, pp. 323–330, Jan. 2005.
- [14] H. He and J. A. Starzyk, "A self-organizing learning array system for power quality classification based on wavelet transform," *IEEE Trans. Power Del.*, vol. 21, no. 1, pp. 286–295, Jan. 2006.

- [15] J. Huang, Z. Jiang, L. Rylands, and M. Negnevitsky, "SVM-based PQ disturbance recognition system," *IET Gener., Transmiss. Distrib.*, vol. 12, no. 2, pp. 328–334, Jan. 2018.
- [16] W.-M. Lin, C.-H. Wu, C.-H. Lin, and F.-S. Cheng, "Detection and classification of multiple power-quality disturbances with wavelet multiclass SVM," *IEEE Trans. Power Del.*, vol. 23, no. 4, pp. 2575–2582, Oct. 2008.
- [17] N. Senroy, S. Suryanarayanan, and P. F. Ribeiro, "An improved Hilbert–Huang method for analysis of time-varying waveforms in power quality," *IEEE Trans. Power Syst.*, vol. 22, no. 4, pp. 1843–1850, Nov. 2007.
- [18] S. Alshahrani, M. Abbod, and G. Taylor, "Detection and classification of power quality disturbances based on Hilbert–Huang transform and feed forward neural networks," in *Proc. 51st Int. Universities Power Eng. Conf. (UPEC)*, Coimbra, Sep. 2016, pp. 1–6.
- [19] P. Janik and T. Lobos, "Automated classification of power-quality disturbances using SVM and RBF networks," *IEEE Trans. Power Del.*, vol. 21, no. 3, pp. 1663–1669, Jul. 2006, doi: [10.1109/TPWRD.2006.874114](https://doi.org/10.1109/TPWRD.2006.874114).
- [20] Z. Liu, Y. Cui, and W. Li, "A classification method for complex power quality disturbances using EEMD and rank wavelet SVM," *IEEE Trans. Smart Grid*, vol. 6, no. 4, pp. 1678–1685, Jul. 2015.
- [21] S. Naderian and A. Salemnia, "Method for classification of PQ events based on discrete Gabor transform with FIR window and T2FK-based SVM and its experimental verification," *IET Gener., Transmiss. Distrib.*, vol. 11, pp. 133–141, Jan. 2017.
- [22] B. Biswal, M. Biswal, S. Mishra, and R. Jalaja, "Automatic classification of power quality events using balanced neural tree," *IEEE Trans. Ind. Electron.*, vol. 61, no. 1, pp. 521–530, Jan. 2014.
- [23] Z.-L. Gaing, "Wavelet-based neural network for power disturbance recognition and classification," *IEEE Trans. Power Del.*, vol. 19, no. 4, pp. 1560–1568, Oct. 2004.
- [24] M. Valtierra-Rodriguez, R. de Jesus Romero-Troncoso, R. A. Osornio-Rios, and A. Garcia-Perez, "Detection and classification of single and combined power quality disturbances using neural networks," *IEEE Trans. Ind. Electron.*, vol. 61, no. 5, pp. 2473–2482, May 2014.
- [25] S. Gunal, O. N. Gerek, D. G. Ece, and R. Edizkan, "The search for optimal feature set in power quality event classification," *Exp. Syst. Appl.*, vol. 36, no. 7, pp. 10266–10273, Sep. 2009.
- [26] U. Singh and S. N. Singh, "A new optimal feature selection scheme for classification of power quality disturbances based on ant colony framework," *Appl. Soft Comput.*, vol. 74, pp. 216–225, Jan. 2019.
- [27] Y. Deng, L. Wang, H. Jia, X. Tong, and F. Li, "A sequence-to-sequence deep learning architecture based on bidirectional GRU for type recognition and time location of combined power quality disturbance," *IEEE Trans. Ind. Informat.*, vol. 15, no. 8, pp. 4481–4493, Aug. 2019.
- [28] Y. Deng, H. Jia, P. Li, X. Tong, and F. Li, "A deep learning method based on long short term memory and sliding time window for type recognition and time location of power quality disturbance," in *Proc. Chin. Autom. Congr. (CAC)*, Xi'an, China, Nov. 2018, pp. 1764–1768.
- [29] F. Zhang, B. Du, and L. Zhang, "Saliency-guided unsupervised feature learning for scene classification," *IEEE Trans. Geosci. Remote Sens.*, vol. 53, no. 4, pp. 2175–2184, Apr. 2015.
- [30] M. Liu, Y. Chen, Z. Zhang, and S. Deng, "Classification of power quality disturbance using segmented and modified S-transform and DCNN-MSVM hybrid model," *IEEE Access*, vol. 11, pp. 890–899, 2023, doi: [10.1109/ACCESS.2022.3233767](https://doi.org/10.1109/ACCESS.2022.3233767).
- [31] N. Rahal, M. Tounsi, A. Hussain, and A. M. Alimi, "Deep sparse auto-encoder features learning for Arabic text recognition," *IEEE Access*, vol. 9, pp. 18569–18584, 2021, doi: [10.1109/ACCESS.2021.3053618](https://doi.org/10.1109/ACCESS.2021.3053618).
- [32] L. Lin, D. Wang, S. Zhao, L. Chen, and N. Huang, "Power quality disturbance feature selection and pattern recognition based on image enhancement techniques," *IEEE Access*, vol. 7, pp. 67889–67904, 2019, doi: [10.1109/ACCESS.2019.2917886](https://doi.org/10.1109/ACCESS.2019.2917886).
- [33] T. Hofmann, J. Puzicha, and J. M. Buhmann, "Unsupervised texture segmentation in a deterministic annealing framework," *IEEE Trans. Pattern Anal. Mach. Intell.*, vol. 20, no. 8, pp. 803–818, Aug. 1998.
- [34] P. Rai and P. Khanna, "A gender classification system robust to occlusion using Gabor features based (2D)2PCA," *J. Vis. Commun. Image Represent.*, vol. 25, no. 5, pp. 1118–1129, Jul. 2014.
- [35] J. K. Kamarainen, V. Kyrki, and H. Kalviainen, "Local and global Gabor features for object recognition," *Pattern Recognit. Image Anal.*, vol. 17, pp. 93–105, 2007, doi: [10.1134/S1054661807010117](https://doi.org/10.1134/S1054661807010117).
- [36] D. Gabor, "Theory of communication. Part 1: The analysis of information," *J. Inst. Electr. Engineers III, Radio Commun. Eng.*, vol. 93, no. 26, pp. 429–441, Nov. 1946.
- [37] J. Feng, L. Liu, X. Cao, L. Jiao, T. Sun, and X. Zhang, "Marginal stacked autoencoder with adaptively-spatial regularization for hyperspectral image classification," *IEEE J. Sel. Topics Appl. Earth Observ. Remote Sens.*, vol. 11, no. 9, pp. 3297–3311, Sep. 2018.
- [38] A. J. Larrazabal, C. Martinez, B. Glocker, and E. Ferrante, "Post-DAE: Anatomically plausible segmentation via post-processing with denoising autoencoders," *IEEE Trans. Med. Imag.*, vol. 39, no. 12, pp. 3813–3820, Dec. 2020.
- [39] X. Ye and Q. Zhu, "Class-incremental learning based on feature extraction of CNN with optimized softmax and one-class classifiers," *IEEE Access*, vol. 7, pp. 42024–42031, 2019, doi: [10.1109/ACCESS.2019.2904614](https://doi.org/10.1109/ACCESS.2019.2904614).
- [40] A. M. Gaouda, M. M. A. Salama, M. R. Sultan, and A. Y. Chikhani, "Power quality detection and classification using wavelet-multiresolution signal decomposition," *IEEE Trans. Power Del.*, vol. 14, no. 4, pp. 1469–1476, Oct. 1999.
- [41] H. HaesAlhelou, H. Parthasarathy, N. Nagpal, V. Agarwal, H. Nagpal, and P. Siano, "Decentralized stochastic disturbance observer-based optimal frequency control method for interconnected power systems with high renewable shares," *IEEE Trans. Ind. Informat.*, vol. 18, no. 5, pp. 3180–3192, May 2022, doi: [10.1109/THI.2021.3107396](https://doi.org/10.1109/THI.2021.3107396).
- [42] J. Liu, H. Song, H. Sun, and H. Zhao, "High-precision identification of power quality disturbances under strong noise environment based on FastICA and random forest," *IEEE Trans. Ind. Informat.*, vol. 17, no. 1, pp. 377–387, Jan. 2021, doi: [10.1109/THI.2020.2966223](https://doi.org/10.1109/THI.2020.2966223).
- [43] L. Fu, T. Zhu, G. Pan, S. Chen, Q. Zhong, and Y. Wei, "Power quality disturbance recognition using VMD-based feature extraction and heuristic feature selection," *Appl. Sci.*, vol. 9, no. 22, p. 4901, Nov. 2019, doi: [10.3390/app9224901](https://doi.org/10.3390/app9224901).
- [44] A. M. Gargoom, N. Ertugrul, and W. L. Soong, "Automatic classification and characterization of power quality events," *IEEE Trans. Power Del.*, vol. 23, no. 4, pp. 2417–2425, Oct. 2008, doi: [10.1109/TPWRD.2008.923998](https://doi.org/10.1109/TPWRD.2008.923998).
- [45] J. Li, Z. Teng, Q. Tang, and J. Song, "Detection and classification of power quality disturbances using double resolution S-transform and DAG-SVMs," *IEEE Trans. Instrum. Meas.*, vol. 65, no. 10, pp. 2302–2312, Oct. 2016.
- [46] X. Shi, H. Yang, Z. Xu, X. Zhang, and M. R. Farahani, "An independent component analysis classification for complex power quality disturbances with sparse auto encoder features," *IEEE Access*, vol. 7, pp. 20961–20966, 2019.
- [47] T. Chakravorti and P. K. Dash, "Multiclass power quality events classification using variational mode decomposition with fast reduced kernel extreme learning machine-based feature selection," *IET Sci., Meas. Technol.*, vol. 12, no. 1, pp. 106–117, Jan. 2018.
- [48] H. He and J. A. Starzyk, "A self-organizing learning array system for power quality classification based on wavelet transform," *IEEE Trans. Power Del.*, vol. 21, no. 1, pp. 286–295, Jan. 2006.
- [49] J. Huang, Z. Jiang, L. Rylands, and M. Negnevitsky, "SVM-based PQ disturbance recognition system," *IET Gener., Transmiss. Distrib.*, vol. 12, no. 2, pp. 328–334, Jan. 2018.
- [50] Z. Liu, Y. Cui, and W. Li, "A classification method for complex power quality disturbances using EEMD and rank wavelet SVM," *IEEE Trans. Smart Grid*, vol. 6, no. 4, pp. 1678–1685, Jul. 2015.



PORAS KHETARPAL received the M.Tech. degree in power electronics, electrical machines and drives from IIT Delhi. He is currently an Assistant Professor with the Information Technology Department, Bharati Vidyapeeth's College of Engineering (Affiliated to Guru Gobind Singh Indraprastha University), New Delhi, India. He has published more than 20 research papers in reputed journals and conferences. His research interests include artificial intelligence and machine learning. He has received the Research Excellence Award from Delhi Technological University, New Delhi, in 2021.



NEELU NAGPAL (Senior Member, IEEE) received the bachelor's degree in electrical engineering from the Delhi College of Engineering, the master's degree (Hons.) in control and instrumentation from Delhi University, and the Ph.D. degree in electrical engineering from Delhi Technological University, Delhi, India. She is presently working as an Associate Professor in EEE Department of Maharaja Agrasen Institute of Technology, Delhi (affiliated to GGSIP University, Delhi). She has grant of one Australian patent. Her research interests include stochastic and nonlinear control, state estimation, smart grid technologies, renewable energy integration, and artificial intelligence. She was a recipient of the Commendable Research Award from Delhi Technological University, during her Ph.D. course. She is the Vice-Chair of the 2023 IEEE Smart Cities Ambassador Program.



MOHAMMED S. AL-NUMAY (Senior Member, IEEE) was born in Riyadh, Saudi Arabia. He received the B.S. degree (Hons.) in electrical engineering from King Saud University, Riyadh, in 1986, the M.S. degree in electrical engineering from Michigan State University, East Lansing, MI, USA, in 1990, and the Ph.D. degree in electrical engineering from the Georgia Institute of Technology, Atlanta, GA, USA, in 1997. Since 1998, he has been with the Electrical Engineering Department, College of Engineering, King Saud University, where he is currently a Full Professor. From 2002 to 2006, he was the Dean of admissions and registration with King Saud University. He is a board member of two universities and four private colleges. In January 2018, he became the Vice President of Educational and Academic Affairs, King Saud University. His research interests include the modeling and control of switched mode power supplies, computer science, renewable energy, and the applications of AI.



PIERLUIGI SIANO (Senior Member, IEEE) received the M.Sc. degree in electronic engineering and the Ph.D. degree in information and electrical engineering from the University of Salerno, Salerno, Italy, in 2001 and 2006, respectively. Since 2021, he has been a Distinguished Visiting Professor with the Department of Electrical and Electronic Engineering Science, University of Johannesburg. He is currently a Professor and the Scientific Director of the Smart Grids and Smart Cities Laboratory, Department of Management and Innovation Systems, University of Salerno. His research interests include demand response, energy management, the integration of distributed energy resources in smart grids, electricity markets, and the planning and management of power systems. In these research fields, he has coauthored more than 700 articles, including more than 410 international journals that received in Scopus more than 17900 citations with an H-index equal to 64. From 2019 to 2022, he was awarded as a Highly Cited Researcher in Engineering by Web of Science Group. He has been the Chair of the IES TC on Smart Grids. He is an Editor of the Power and Energy Society Section of IEEE ACCESS, IEEE TRANSACTIONS ON POWER SYSTEMS, IEEE TRANSACTIONS ON INDUSTRIAL INFORMATICS, IEEE TRANSACTIONS ON INDUSTRIAL ELECTRONICS, and IEEE SYSTEMS JOURNAL.



YOGENDRA ARYA (Senior Member, IEEE) is currently an Associate Professor with the Department of Electrical Engineering, J. C. Bose University of Science and Technology, YMCA, Faridabad, India. He has published more than 50 research articles in reputed international journals. His research interest includes power system operation and control. He is a fellow of IETE. He has placed among top 2% of researchers by Stanford University, USA, in 2019, 2020, and 2021. He is an academic/associate editor of few SCIE journals.



NEELAM KASSARWANI received the degree in electrical engineering from Madan Mohan Malviya Engineering College, Gorakhpur, India, the master's degree in power systems (power system apparatus) from Delhi University, and the Ph.D. degree in electrical engineering from the National Institute of Technology, Kurukshetra, India. She is presently working as an Associate Professor in EEE Department of Maharaja Agrasen Institute of Technology, Delhi, (affiliated to GGSIP University, Delhi). From 1980 to 1987, she was a National Scholarship Holder for her education. She has 20 years of experience in teaching and ten years of experience in industrial. She has eight research publications in international journals and conferences. Her research interests include power system modeling and control, power quality, dynamic voltage restore, artificial intelligence, and renewable energy systems.

...